Hindawi Publishing Corporation
Mathematical Problems in Engineering
Volume 2014, Article ID 856272, 8 pages
http://dx.doi.org/10.1155/2014/856272

Research Article

Experimental and Numerical Analysis of Stainless Steel Microtube in Flaring Process

Tsung-Chia Chen and Wei-Kai Ceng

National Chin-Yi University of Technology, No. 57, Section 2, Zhongshan Road, Taiping District, Taichung 41170, Taiwan

Correspondence should be addressed to Tsung-Chia Chen; ctchen@ncut.edu.tw

Received 14 February 2014; Accepted 4 April 2014; Published 14 May 2014

Academic Editor: Her-Terng Yau

This study, with experiments and comparisons, aims to analyze the difference of stainless (SUS316L) microtubes in the flaring forming among dies with various semicone angles (35°, 40°, 45°, 50°, and 55°). The flow rule by Prandtl-Reuss combined with the finite element deformation theory and updated Lagrangian formulation (ULF) is applied to establish the finite element analysis equation for an incremental elastoplastic deformation to simulate the microtube flaring process. The broad $r_{\min}$ algorithm is utilized in the forming process for the elastoplastic state and die contact. The simulation data allow acquiring the deformation traceability, the relationship between punch load and punch stroke, the distribution of stress and strain, the distribution of the thinnest thickness resulted from dies with different semicone angles, and the distribution of flaring radius caused by dies with distinct semicone angles in the forming process. The experimental result presents similar results to the relationship between punch load and punch stroke and the simulation of the coefficient of friction $\mu = 0.05$, revealing the analysis being suitable for the analysis of microtube cone angle flaring process. The analysis and experimental results show that the thinnest thickness of the microtube increases with increasing semicone angles of dies and the maximal flaring radius of microtubes increases with increasing semicone angles of dies.

1. Introduction

The rapid development of modern industries has accelerated the progress of material processing, in which stamping technique that could largely enhance manufacturing accuracy and production efficiency cannot be neglected. Moreover, stamping would replace drilling or milling for the materials suitable for stamping. The development factors in stamping aims not to proceed processing at the final shape of components and it is regarded as the optimal cost-reduction processing in modern industries and presents various technological and economic advantages. Stamping is mostly applied to large batch production, which relies on more complicated and expensive die techniques. However, the cost could be reduced because of the large batch production. Materials are likely to show fracture, local overthinning, or wrinkling because of unfavorable forming or bad settings of processing parameters in stamping. To reduce such defects, various factors need to be taken into account and be broken through in stamping. Furthermore, when the outer force is removed and the elasticity tends to be recovered in stamping, merely a part of it would be recovered because of the restriction of plasticity. Such recovery is called springback, in which elasticity and plasticity are balanced. Factors in elasticity recovery contain the hardness, bend radius, and curvature of materials. The rapid development of microelectromechanical system (MEMS) in the past years has microcomponent design be emphasized, and the applications have gradually covered electronics industry and biomedicine industry so that the costs and the production time are largely reduced. The stainless steel SUS316L in Japanese industrial standards (JIS) presents excellent acid endurance and corrosion resistance and it reveals better acid endurance than SUS304 does and could be easily proceeded heat treatment and forming. The products therefore could be applied to the components for chemical processing equipment, nuclear power plant, air-condition storage tank, pipe making, and corrosion resistance occasion.

Makinouchi and Kawka [1] proposed degenerated shell elements and combined them in statically explicit finite element equation to compare distinct integration rules, including complete integration, simplified integration, selective reduced integration, assumed strain field, and stable matrix rule. Mirzai et al. [2] mentioned the importance of microtubes in various domains, where the ductility of micromaterials was one of the key parameters affecting the material forming. They also changed the angles of cone dies in the experiment to analyze the forming limit in the microtube flaring experiment and discovered the increasing flaring limit with increasing cone die angles. Sun and Yang [3] studied the forming limit of the tube axial compression and considered the wrinkling and fracture resulting from round angles and cone angles in order to establish a development standard for plasticity forming with the combination of finite element analysis and forming limit. The effects of feasibility and parameters in the process on the research showed the stable forming of processing parameters being in reasonable range and it was reliable for forming limit. Lu [4] proposed definite theoretical equations to calculate bend angle and strain rate after tube flaring so that the tube flaring resulted from changing the semicone angles of dies. The result revealed the larger semicone angle resulting in the deeper stroke and the material flow rate was better. Almeida et al. [5] designed dies with different cone angles for the experiments of necking and flaring, compared the results with finite element analysis, and changed the coefficient of friction to achieve the best forming and reduce the product wrinkling. The result presented that the ductility fracture analysis could accurately evaluate the reliability of tube in the flaring and necking process.

Regarding the analysis of microtube flaring in this study, the products could be applied to the relative components, such as industrial products of innerplate of airplane, wire protection tube of electronic equipment, and line connection and general home electric appliances, and electronic components for assembly or welding. For the microtube cone angle flaring, the designed die is covered with the microtube so that the microtube moves down to the semicone angle of the die with punch stamping. With the pressing of punch, the microtube shows flaring because of the semicone angle of the die. When stamping to certain extent, the forming limit would appear that the tube end would reveal thinning and wrinkling. In this case, the microtube forming analysis is simulated in advance in order to prevent tube end flaring from fracture because of too much stroke. The stroke therefore is set a fixed value in the simulation process, and punch load, deformation traceability, stress figure, strain figure, and forming thickness distribution are further discussed and calculated the strength with numerical simulation to shorten the developing time. It aims to achieve the optimization of cost reduction and product quality enhancement.

2. Basic Theory

2.1. Basic Hypothesis. The blank considered in this study is made several assumptions in the elastoplastic deformation.

(1) The material is assumed homogeneous.

(2) The material is assumed planar anisotropic.

(3) The material satisfies Hooke's law in the elasticity area.

(4) Dies are regarded as the rigid body.

(5) The effect of residual stress is not considered in the material forming.

(6) The effect of temperature is not considered in the material forming.

2.2. Evolution of Principle. A governing equation suitable for various metal forming processes is deducted with the stress-stress rate relationship in metal material deformation, ULF in finite deformation, and the material composition. Jaumann differential of Cauchy stress is used for the stress rate of the constitutive equation and updating principle of virtual work formed by Lagrangian could omit the volume function and the equation could be revised as follows [6]:

$$\int_{V^E} \left(\mathring{\sigma}_{ij} - 2\sigma_{ik}\dot{\varepsilon}_{kj}\right) \delta\dot{\varepsilon}_{ij} dV + \int_{V^E} \sigma_{jk} L_{ik} \delta L_{ij} dV = \int_{S_f} \dot{f} \delta v_i \, dS. \tag{1}$$

The common equations in finite element are also included:

$$\{v\} = [N]\left\{\dot{d}\right\}, \quad \{\dot{\varepsilon}\} = [B]\left\{\dot{d}\right\}, \quad \{L\} = [E]\left\{\dot{d}\right\}, \tag{2}$$

where $[N]$ is the shape function, $\{\dot{d}\}$ the nodal velocity, $[B]$ the strain rate-velocity matrix, and $[E]$ the velocity gradient-velocity matrix. With finite element discretization, the rigid governing equation for large deformation is shown as below:

$$[K]\{\Delta u\} = \{\Delta F\}, \tag{3}$$

where

$$[K] = \sum_{\langle E\rangle} \int_{V^E} [B]^T \left([C^{\mathrm{ep}}] - [Q]\right)[B]\, dV + \sum_{\langle E\rangle} \int_{V^E} [E]^T [Z]\, [E]\, dV \tag{4}$$

and K is generally regarded as the overall elastoplastic stiffness matrix, $\{\Delta u\}$ the nodal displacement increment, $\{\Delta F\}$ the nodal force increment, $[Q]$ and $[Z]$ the stress modified matrix, and $[C^{\mathrm{ep}}]$ the elastoplastic stress-strain matrix.

2.3. Brief Introduction of Selective Reduced Integration (SRI). The volume of a plastic object is uncompressible. To satisfy the integration, more restrictions are required for the elements on the thin plate. Such a phenomenon would result in

the shear strains γ_{xz} and γ_{yz} of the thin plate element being set 0 during the deformation [7]. It is proven that selective reduced integration (SRI) could effectively deal with such uncompressible volume [8]. Selective reduced integration has been clearly described in the finite element developed by Hughes [9].

2.4. Scale Factor for Sheet Metal Microforming Process. The size effect can be neglected when the thickness of the sheet metal is larger than 1.0 mm, whereas the size effect is crucial when the thickness is less than 1.0 mm. The thickness of sheet metals is in the micron range in the microforming process; therefore, the size effect makes the traditional material model unsuitable for microforming processes. Consequently, a new material model must be established for microstamping process. The traditional swift material model (without considering size effect) is first applied in this study. Consider

$$\overline{\sigma} = K\left(\varepsilon_0 + \overline{\varepsilon_p}\right)^n. \tag{5}$$

The applied sheet metal thickness is 150 μm, which is regarded as a microforming process considering the size effect. The thickness of sheet metal is considered in the traditional material model for the amendment of stress–strain relations. Consequently, (5) is amended as follows:

$$\overline{\sigma}\,(t, \overline{\varepsilon}) = aKe^{bt}\left(\varepsilon_0 + \overline{\varepsilon_p}\right)^{n(ce^{dt}-1)}, \tag{6}$$

where a, b, c, and d are the correction values and t is the sheet thickness.

The values for a, b, c, and d, obtained from the research results of Peng et al. [10], are substituted in (6). Subsequently,

$$\overline{\sigma}\,(t, \overline{\varepsilon}) = 0.73667Ke^{0.3152t}\left(\varepsilon_0 + \overline{\varepsilon_p}\right)^{n(1.0106e^{-0.01029t}-1)}. \tag{7}$$

Finite element analysis is conducted for the modified material model (7) in this study. Experiments are further implemented to verify the credibility of the modified material models.

3. Experimental and Numerical Analysis

Applying the shell elements of the four nodes of a quadrangle to deducting the stiffness matrix, which is processed with CAD, the established tube shape is proceeded mesh segmentation, which is transformed into data files for the numerical analysis in the elastoplastic 3D finite element. The simulated results are output to CAD for analyses, in which the deformation diagram and the strain distribution could be displayed. Regarding the parameter change, the die semicone angle is changed to discuss the relations between punch load and punch stroke, the distribution of maximal stress and maximal strain, the thickness distribution, and the maximal radius after the flaring.

In the semicone angle flaring, the difference between the simulation results of the modified material model and the experimental results is discussed, and the microtube flaring deformation is observed. Figure 1 shows the microtube size and the tool allocation, and Figure 2 displays the mesh distribution used in the numerical analysis.

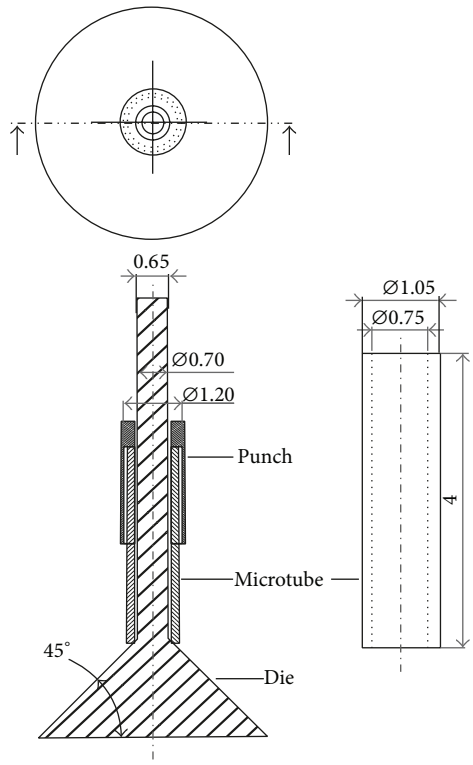

Figure 1: Microtube size and tools allocation.

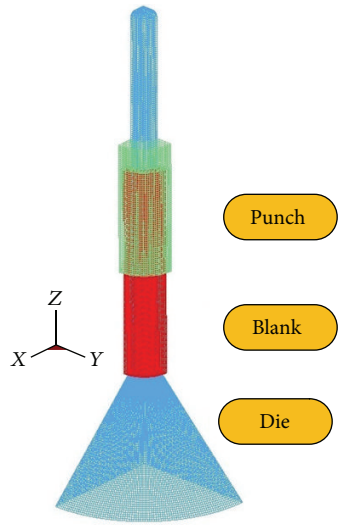

Figure 2: Mesh allocation used in the numerical analysis.

3.1. Experimental Equipment. A 10 kN microelectronic press (Figure 3), the data-acquisition equipment, a tool covering punch, blank holder, and semicone angle of 45° die are contained for this study. In order to reduce the coefficient of friction in the die, dry lubricant zinc stearate powder is used in the experiment. The tool components and the tool set-up for the microtube flaring are shown in Figures 4 and 5, respectively.

Figure 3: Microelectronic press.

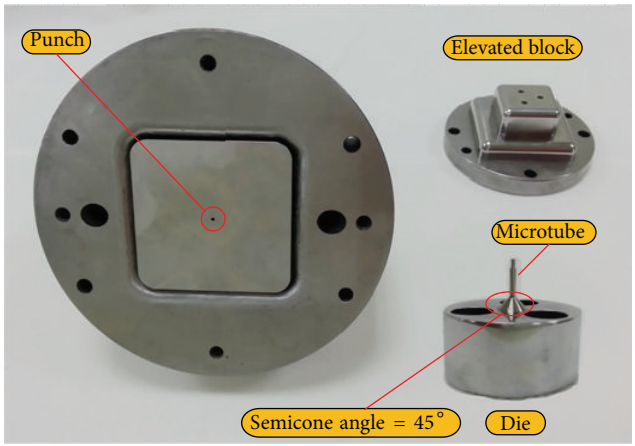

Figure 4: Tool components.

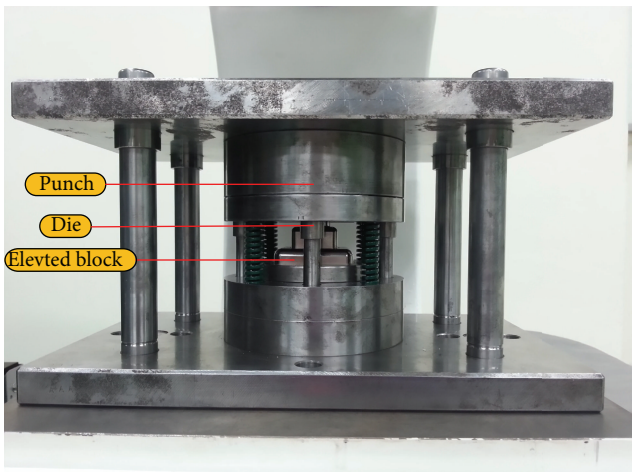

Figure 5: Tools set-up.

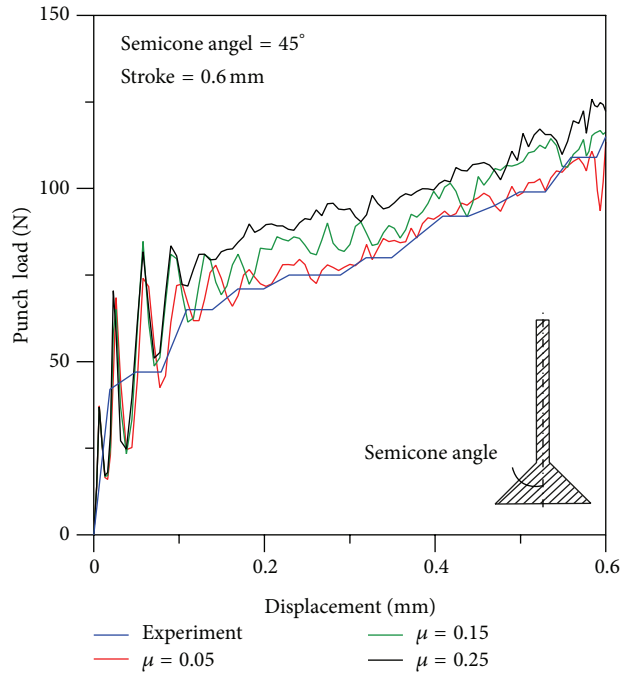

Figure 6: Effects of coefficient of friction on punch load.

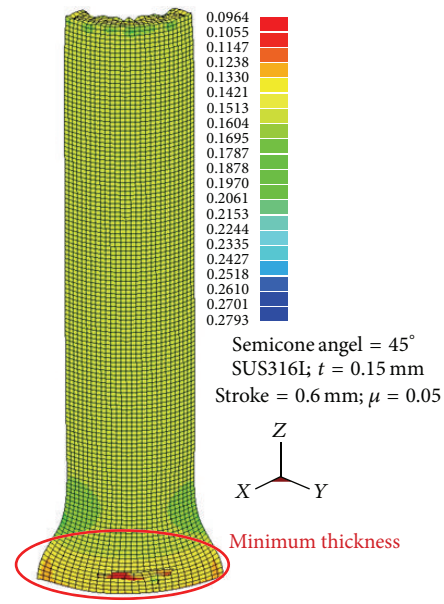

Figure 7: Thickness distribution.

3.2. Boundary Condition. In the microstamping process, the blank would contact with punch and the contact of nodes would change with the blank deformation. For this reason, when calculating the displacement increment, the contacted nodes need to check the normal component of nodal force being less than or equal to 0. If so, the boundary condition of the node in the next displacement increment needs to be changed into the boundary conditions of free nodes. The original free node also needs to check the geometric position

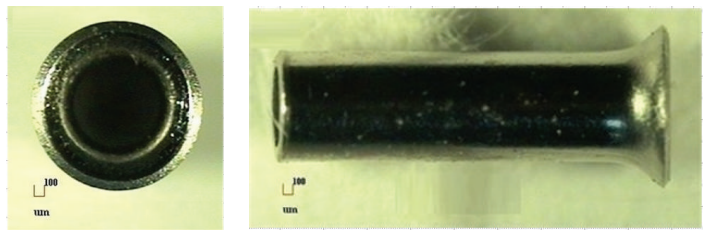

(a) (b)

Figure 8: Experimental product of microtube: (a) bottom view and (b) side view.

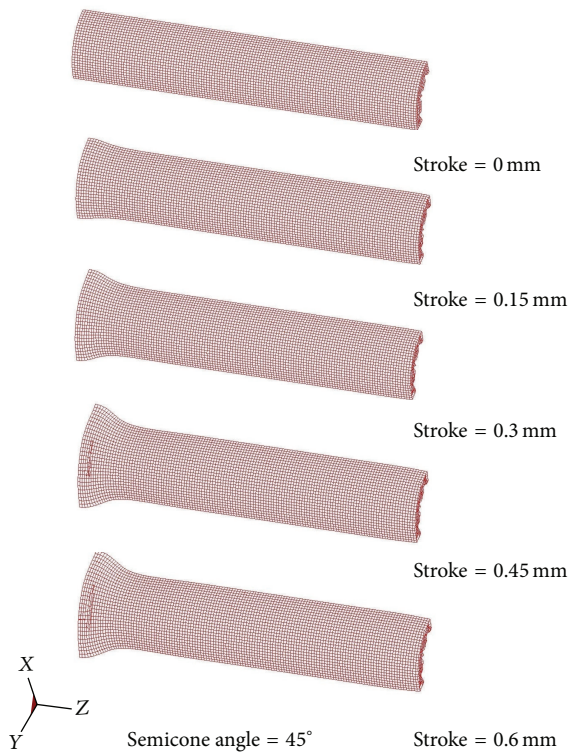

Figure 9: Deformation traceability at the semicone angle of 45°.

being contacted with the die. If so, the boundary condition of the node would be changed into the boundary condition of the contacted node in the following displacement increment calculation. The above calculation is the treatment with broad $r_{\min}$ rules.

All contact surfaces are generated in the alternation between sliding and viscous friction that calculation difficulties would cause. The conditions for friction therefore need to be emphasized. Oden and Pires [11] and Saran and Wagoner [12] proposed modified coulomb friction rule, in which the friction with sliding and viscosity was covered. Such a friction rule effectively solved the problem of discontinuous sliding directions. The simulation conditions in this microstamping process assume the coefficient of friction $\mu = 0.05$, 0.15, and 0.25 for the comparisons with the experimental values.

Table 1: Microtube material parameter (unit: mm).

Material	E (Gpa)	σ_y (MPa)	K(MPa)	n	ε_0
SUS316L	358	287	1404.88	0.582	0.077

The true stress-strain curve is approximated by $\overline{\sigma}(t, \overline{\varepsilon}) = 0.73667Ke^{0.3152t}(\varepsilon_0 + \overline{\varepsilon_p})^{n(1.0106e^{-0.01029t}-1)}$; $\nu = 0.3$; E: Young's modulus; and σ_y: yield stress.

3.3. Elastoplastic Treatment. The blank being elastic or plastic in the increasing deformation needs to be judged so that the elements remain the same at each increment. The $r_{\min}$ rule is also applied to the judgment of elastoplastic state.

3.4. Unloading Treatment. Springback is a critical factor in microstamping processes; therefore, the unloaded behaviors in the microtube flaring process should be taken into account. When the tool is completely removed, the springback is calculated and the boundary condition of a new power is assigned to the contacted node, set as $\Delta f = -f$.

4. Result and Discussion

The changes of die semicone angles, 35°, 40°, 45°, 50°, and 55°, are discussed to analyze the microtube flaring process. The microtube material is SUS316L, and the material parameters for the numerical simulation analysis are the traditional material parameters modified with (7), where K is 1404.88 Mpa and n is 0.582, Table 1.

4.1. Comparison of Microtube Flaring Experiment and Simulation. Figure 6 shows the numerical simulation analysis of the die semicone angle of 45° with the changes of the coefficient of friction $\mu = 0.05$, 0.15, and 0.25. The results are compared with the stroke-punch load relationship acquired in the experiment and the relationship is close to the experiment curve when the coefficient of friction $\mu = 0.05$. The coefficient of friction $\mu = 0.05$ is therefore used for the numerical simulation analysis. Furthermore, when the stroke = 0.65 mm (die semicone angle of 45°), fracture appears in both experimental and simulated microtube flaring processes. With repeated simulation analyses, the stroke for the semicone angle flaring process is finally set 0.6 mm to analyze the microtube flaring process. From Figure 6, when the die contacts the blank, the punch load significantly increases, the punch pushes the tube

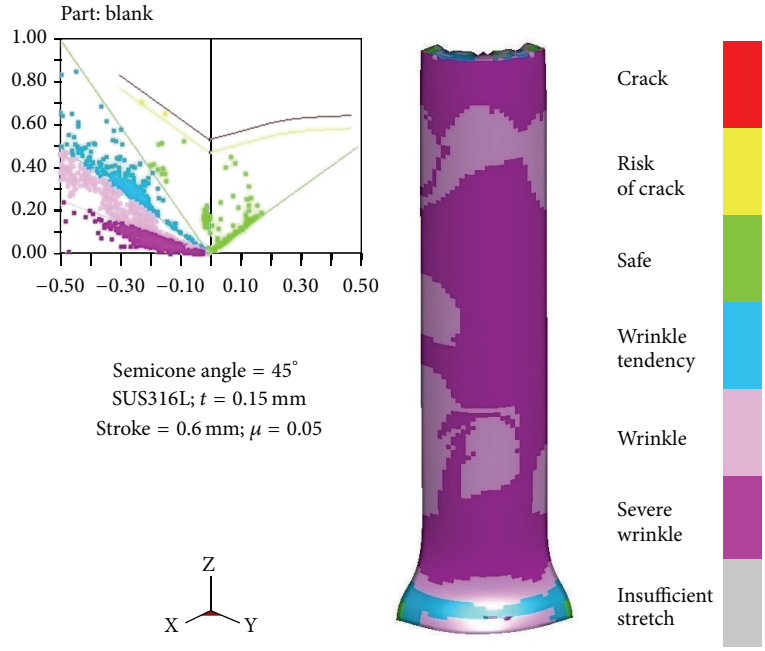

Figure 10: Forming limit at the semicone angle 45°.

to the die semicone angle resulting in tube end flaring because of the punch pressing the microtube, and the punch load increases. Figure 7 shows the thickness distribution after the microtube flaring, in which the thinnest microtube is the microtube flaring after the semicone angle flaring process. Figure 8 displays the experimental product of the microtubes flaring.

4.2. Microtube Flaring Process. Figure 9 shows the geometric deformation of the semicone angle, 45°, microtube flaring, in which the microtube end contacts the die semicone angle to generate flaring deformation because of the punch pressing the stamping. All contacted interfaces are accurately calculated through $r_{\min}$ rules.

Figure 10 displays the semicone angle, 45°, forming limit. With finite element analysis, the complete deformation of the microtube flaring could be accurately analyzed, and the fracture of the blank could be realized. The stroke is set 0.6 mm in this study in order to avoid the tube end fracture caused by lengthy stroke. The microtube could bear different maximal stroke because of distinct die semicone angles.

4.3. Effects of Die Semicone Angle on Punch Load. Figure 11 presents the stroke-punch load relationship from the changes of die semicone angles, in which the punch load increases with increasing die semicone angle in the cone angle flaring process.

4.4. Effects of Die Semicone Angle on the Thinnest Thickness. Figure 12 shows the relationship between distinct die semicone angles and microtube thickness, in which the larger die semicone angle would result in thinner thickness. The even stretch of punch stamping would thin the material in the microtube flaring. The thickness in the figure is the thickness before and after tube springback. The material thickness after springback would slightly increase, and the shape after springback is the final shape of the material plasticity deformation.

4.5. Effects of Die Semicone Angle on Stress and Strain. Figure 13 displays the relationship between different die semicone angles and the maximal stress, whose unit is MPa. The maximal stress increases with increasing die semicone angles and the maximal stress before springback, 1688.486 MPa, appears on the die semicone angle of 55°, while the minimal stress, 1508.335 MPa, appears on the die semicone angle of 35°. After the unload springback, the stress becomes smaller than the one before springback. Figure 14 shows the relationship between different die semicone angles and the maximal strain, whose unit is mm/mm. The maximal strain would increase with increasing die semicone angles, and the strain before springback would be larger than it after springback. The maximal strain before springback, 0.943992 mm/mm, appears on the die semicone angle of 55°, while the minimal strain, 0.734335 mm/mm, is revealed on the die semicone angle of 35°. The maximal strain after springback, 0.941067 mm/mm, presents on the die semicone angle of 55°, while the minimal strain, 0.731818 mm/mm, appears on the die semicone angle of 35°.

4.6. Effects of Die Semi-Cone Angle on Flaring Radius. Figure 15 displays the maximal flaring radius measured after the die semicone angle flaring, in which the maximal flaring radius increases with increasing die semicone angles. However, the material shows fracture at the die semicone angles of 50° and 55° when the stroke is 0.6 mm. In this case, the

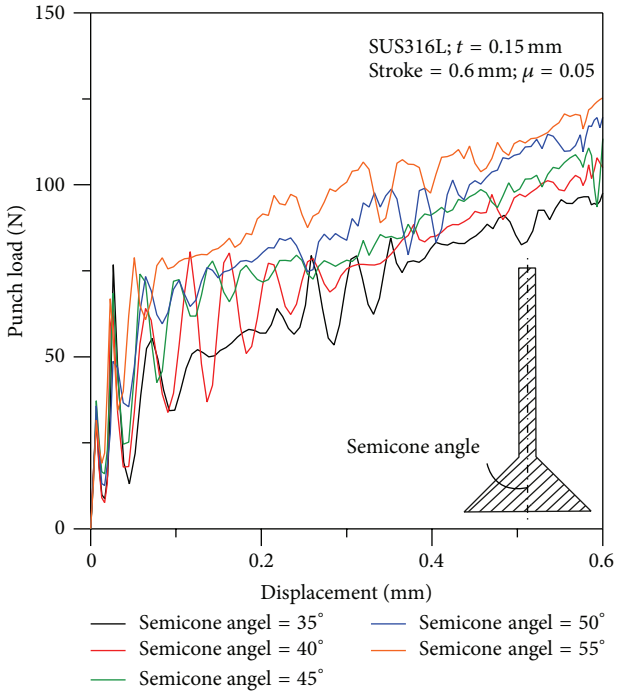

Figure 11: Effects of die semicone angle on punch load.

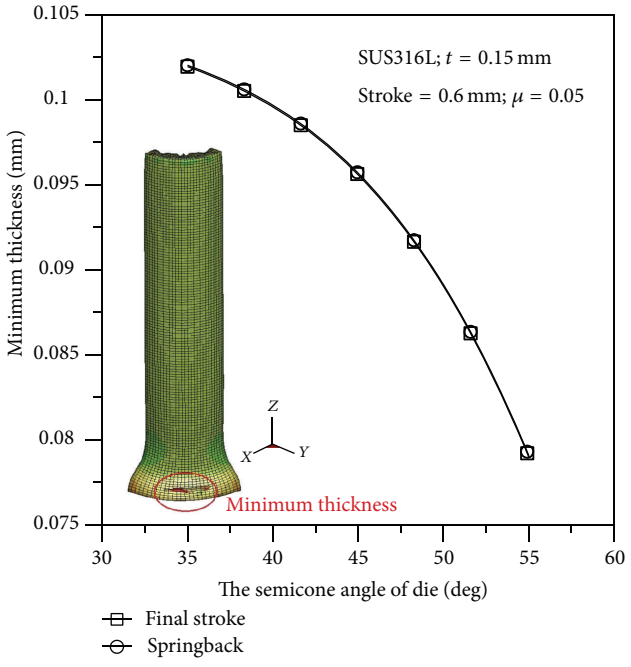

Figure 12: Effects of die semicone angle on the thinnest thickness.

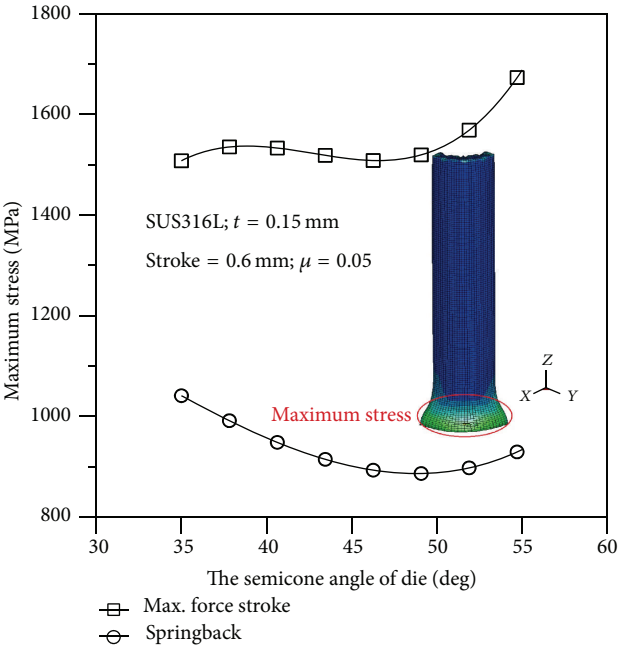

Figure 13: Effects of die semicone angles on the maximal stress.

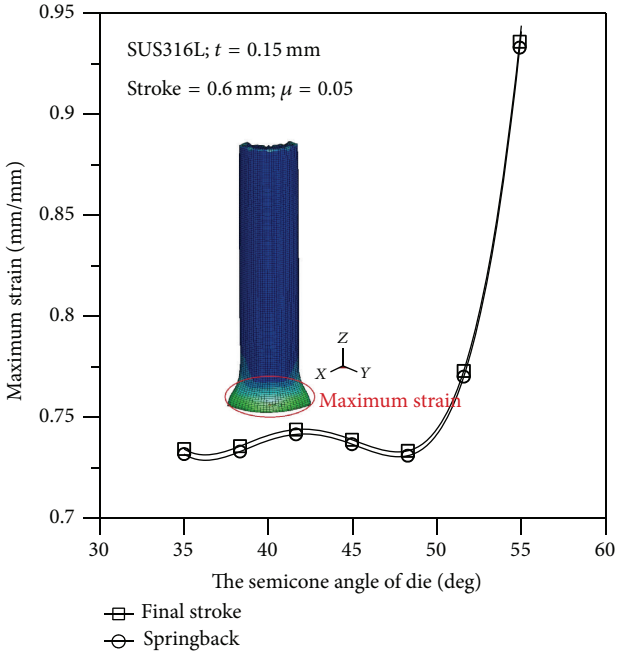

Figure 14: Effects of die semicone angles on the maximal strain.

maximal flaring radius would decrease at the semicone angles of 50° and 55°. Besides, the maximal flaring radius measured after springback reveals slight changes.

5. Conclusion

Elastoplastic deformation finite element analysis is utilized for the calculation in this study, and selective reduced integration (SRI) is applied to develop the microforming simulation of metal-plate. The nonlinear treatment is calculated with an increment, and $r_{\min}$ is used for restricting the gap between the increments so that the calculation presents linear relationship. The simulation of microtube flaring with finite element is concluded as below.

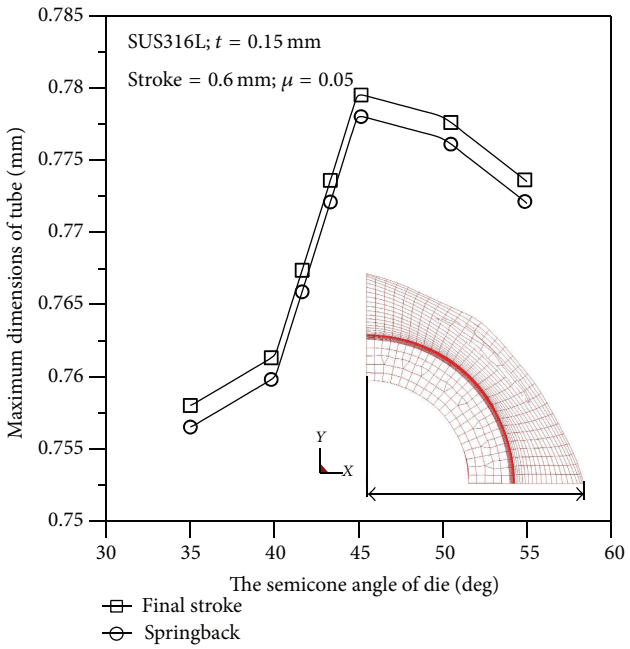

Figure 15: Effects of die semicone angles on the maximal flaring radius.

(1) The finite element analysis could accurately analyze the complete deformation of the microtube flaring and it conforms to the experimental result.

(2) The material with large die semicone angle would bear larger punch load than the one with small die semicone angle does.

(3) The thickness after the tube end flaring is thinning with increasing die semicone angles. The thinnest thickness, 0.102166 mm, appears on the die semicone angle of 35°, and the thinnest thickness, 0.079188 mm, shows on the die semicone angle of 55°.

(4) Both stress and strain increase with increasing die semicone angles.

(5) In the microtube flaring simulation, the thinnest thickness of the material slightly increases after the unload springback, and the stress would largely decrease, while the strain slightly decreases.

(6) The maximal flaring radius of the microtube end increases with increasing die semicone angles.

Conflict of Interests

The authors declare that there is no conflict of interests regarding the publication of this paper.

References

[1] A. Makinouchi and M. Kawka, "Process simulation in sheet metal forming," *Journal of Materials Processing Technology*, vol. 46, no. 3-4, pp. 291–307, 1994.

[2] M. A. Mirzai, K. Manabe, and T. Mabuchi, "Deformation characteristics of microtubes in flaring test," *Journal of Materials Processing Technology*, vol. 201, no. 1–3, pp. 214–219, 2008.

[3] Z. C. Sun and H. Yang, "Study on forming limit and feasibility of tube axial compressive process," *Journal of Materials Processing Technology*, vol. 187-188, pp. 292–295, 2007.

[4] Y. H. Lu, "Study of tube flaring ratio and strain rate in the tube flaring process," *Finite Elements in Analysis and Design*, vol. 40, no. 3, pp. 305–318, 2004.

[5] B. P. P. Almeida, M. L. Alves, P. A. R. Rosa, A. G. Brito, and P. A. F. Martins, "Expansion and reduction of thin-walled tubes using a die: experimental and theoretical investigation," *International Journal of Machine Tools and Manufacture*, vol. 46, no. 12-13, pp. 1643–1652, 2006.

[6] R. M. McMeeking and J. R. Rice, "Finite-element formulations for problems of large elastic-plastic deformation," *International Journal of Solids and Structures*, vol. 11, no. 5, pp. 601–616, 1975.

[7] E. Hinton and D. R. Owen, *Finite Element Software for Plates and Shell*, Pineridge, Swansea, UK, 1984.

[8] T. J. R. Hughes, *The Finite Element Method*, Prentice Hall, Englewood Cliffs, NJ, USA, 1987.

[9] T. J. R. Hughes, "Generalization of selective integration procedures to anisotropic and nonlinear media," *International Journal for Numerical Methods in Engineering*, vol. 15, no. 9, pp. 1413–1418, 1980.

[10] L. Peng, F. Liu, J. Ni, and X. Lai, "Size effects in thin sheet metal forming and its elastic-plastic constitutive model," *Materials and Design*, vol. 28, no. 5, pp. 1731–1736, 2007.

[11] J. T. Oden and E. B. Pires, "Nonlocal and nonlinear friction laws and variational principles for contact problems in elasticity," *Transactions of the ASME Journal of Applied Mechanics*, vol. 50, no. 1, pp. 67–76, 1983.

[12] M. J. Saran and R. H. Wagoner, "A consistent implicit formulation for nonlinear finite element modeling with contact and friction. Part I: theory," *Transactions of the ASME Journal of Applied Mechanics*, vol. 58, no. 2, pp. 499–506, 1991.